Phytochemistry 176 (2020) 112395

Contents lists available at ScienceDirect

Phytochemistry

journal homepage: www.elsevier.com/locate/phytochem

Diterpenoids from *Euphorbia royleana* reverse P-glycoprotein-mediated multidrug resistance in cancer cells

Sharpkate Shaker[a,1], Jun Sang[a,1], Xue-Long Yan[a], Run-Zhu Fan[a], Gui-Hua Tang[a], You-Kai Xu[b], Sheng Yin[a,*]

[a] School of Pharmaceutical Sciences, Sun Yat-sen University, Guangzhou, Guangdong, 510006, China
[b] Key Laboratory of Tropical Plant Resources and Sustainable Use, Xishuangbanna Tropical Botanical Garden, Chinese Academy of Sciences, Menglun, Yunnan, 666303, China

ARTICLE INFO

Keywords:
Euphorbiaceae
Euphorbia royleana
Diterpenoids
Multidrug resistance (MDR)
P-glycoprotein

ABSTRACT

Eight previously undescribed diterpenoids, euphoroyleans A – H, including two cembranes, three ingenanes, two *ent*-atisanes, and one *ent*-kaurane, along with 22 known analogues were isolated from the whole plants of *Euphorbia royleana*. The structures of euphoroyleans A – H, including the absolute configurations, were elucidated by extensive spectroscopic analyses, chemical transformation, and single crystal X-ray diffractions. All the isolates were screened for their chemoreversal abilities on P-glycoprotein (P-gp)-mediated multidrug resistance (MDR) cancer cell line HepG2/DOX, and eight compounds exhibited significant activities. Among them, ingol-3,7,12-triacetate-8-benzoate, the most active MDR modulator with no obvious cytotoxicity, could enhance the efficacy of anticancer drug DOX to *ca.* 105 folds at 10 μM, being stronger than the positive drug verapamil. Mechanistic study revealed that ingol-3,7,12-triacetate-8-benzoate could inhibit the transport activity of P-gp rather than its expression, and the possible recognition mechanism between compounds and P-gp was predicted by molecular docking.

1. Introduction

Multidrug resistance (MDR) designates a phenomenon where resistance to one drug is accompanied by resistance to drugs that are structurally and functionally unrelated. Clinically, MDR is considered as one of the leading causes of treatment failure in the chemotherapy of malignant tumors. The main mechanism of MDR is the overproduction of P-glycoprotein (P-gp) in the plasma membranes of resistant cells, where the P-gp acts as an energy-dependent efflux pump, reducing the intracellular accumulation of anticancer drugs (Sarkadi et al., 2006). Thus, compounds with P-gp inhibitory activities are considered as promising MDR reversal agents when coadministered with an anticancer drug in cancer therapy.

Plants of *Euphorbia* (Euphorbiaceae) are a rich source of structurally diverse diterpenoids, namely *Euphorbia* diterpenoids. Until now, more than 700 *Euphorbia* diterpenoids, incorporating over 30 skeletal types, have been isolated from *Euphorbia* plants (Vasas and Hohmann, 2014). Recently, their fascinating structures and MDR reversal activities have attracted considerable interest from related scientific communities (Shi et al., 2008). *Euphorbia royleana* Boiss. is a thorny succulent shrub, distributed in most areas of southwest China. It is known as “Ba Wang Bian” in traditional Chinese medicine (TCM) for the treatment of inflammation and rheumatic pain (Flora of China Editorial Committee, 1997). Previous chemical investigations of this plant led to the isolation of a series of diverse diterpenoids, and some of them exhibited NO inhibitory and antiangiogenic activities (Li et al., 2009; Wang et al., 2019).

As part of our continuing efforts to discover MDR reversal agents from the Euphorbiaceae plants (Zhu et al., 2016; Li et al., 2020; Zhang et al., 2020), eight previously undescribed diterpenoids and 22 known analogues were obtained from the whole plants of *E. royleana*. All of the isolates were evaluated for their chemoreversal activities on P-gp high-expressed HepG2/DOX cells. Herein, the details of isolation, structural elucidation, chemoreversal activities, and related mechanism of these isolates are described.

* Corresponding author.
E-mail address: yinsh2@mail.sysu.edu.cn (S. Yin).
[1] These authors contributed equally to this work.

https://doi.org/10.1016/j.phytochem.2020.112395
Received 7 February 2020; Received in revised form 18 March 2020; Accepted 17 April 2020
Available online 27 April 2020
0031-9422/

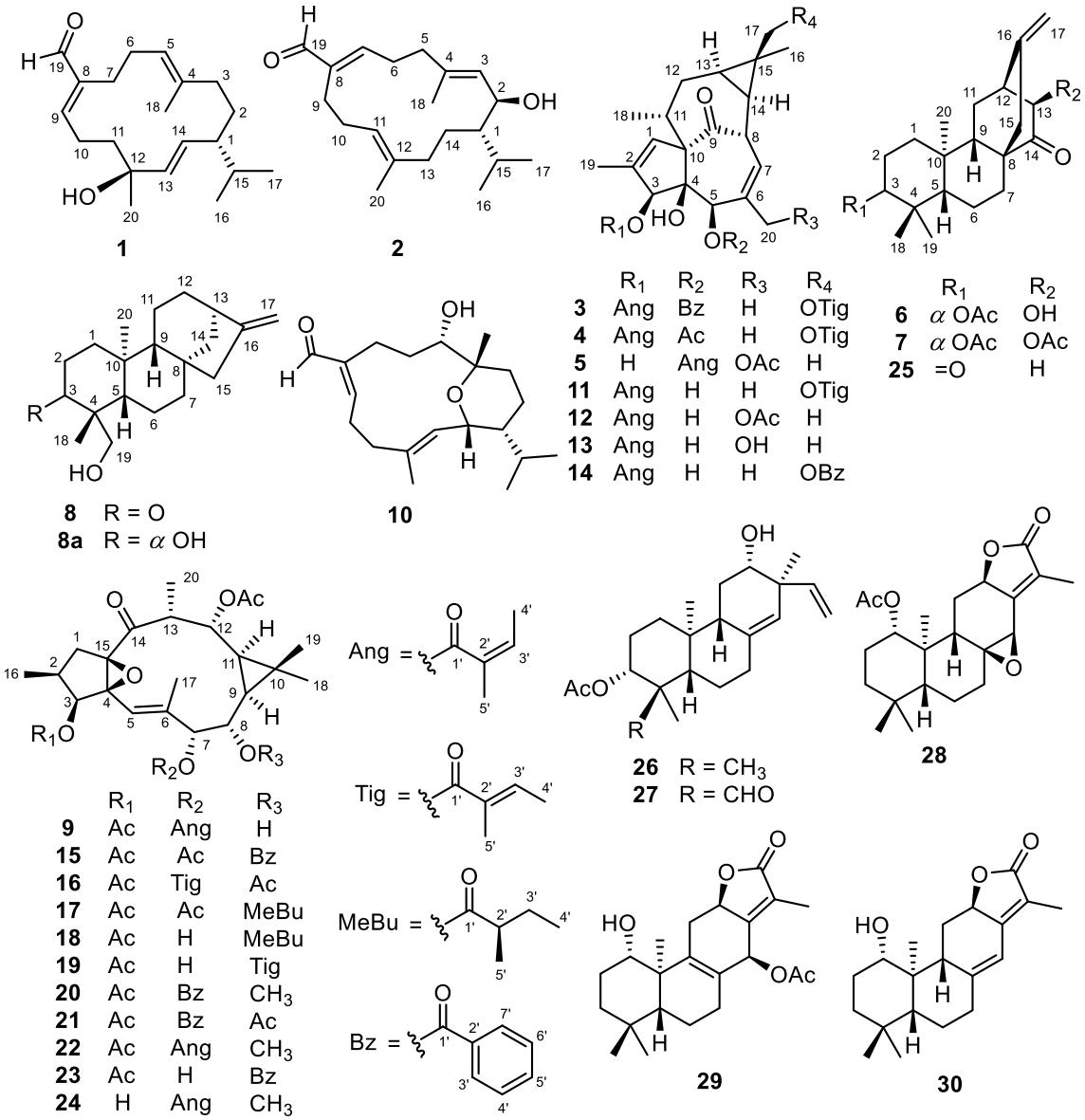

Fig. 1. The structures of compounds **1–30** and **8a**.

2. Results and discussion

2.1. Extraction and structural elucidation

The air-dried powder of the whole plants of *E. royleana* was extracted with 95% EtOH at room temperature to give a crude extract, which was suspended in water and successively partitioned with petroleum ether, EtOAc, and *n*-BuOH. A series of column chromatographic separations of these fractions afforded compounds **1–30** (Fig. 1).

Compound **1** was obtained as colorless crystals. The molecular formula $C_{20}H_{32}O_2$ was determined by the HRESIMS ion peak at *m/z* 327.2289 $[M + Na]^+$ (calcd for $C_{20}H_{32}O_2Na^+$, 327.2295). The IR spectrum displayed absorption bands for hydroxyl (3418 cm^{-1}) and conjugated carbonyl (1664 cm^{-1}) groups. The ^1H NMR data (Table 1) displayed signals for four methyls [δ_H 0.83 (d, J = 6.8 Hz), 0.87 (d, J = 6.8 Hz), 1.42 (s), and 1.54 (s)], four olefinic protons [δ_H 4.83 (d, J = 9.0 Hz), δ_H 5.27 (dd, J = 15.8, 8.8 Hz), δ_H 5.72 (d, J = 15.8 Hz), and δ_H 6.52 (dd, J = 9.9, 4.9 Hz)], a formyl proton [δ_H 9.37 (s)], and a series of aliphatic multiplets. The ^{13}C NMR spectrum, combined with the DEPT experiment resolved 20 carbon resonances attributable to a conjugated aldehyde carbonyl (δ_C 195.5), two trisubstituted double bonds (δ_C 156.0, 142.2, 133.6, and 124.0), a disubstituted double bond (δ_C 136.9 and 130.8), an oxygenated sp^3 tertiary carbon (δ_C 72.6), four methyls, six sp^3 methylenes, and two sp^3 methines. The above-mentioned information was very similar to those of a known cembrane, (1*R*,4*R*,2*E*,7*E*,11*E*)-cembra-2,7,11-trien-4-ol (Bowden et al., 1981), with the only difference being the replacement of a vinyl-methyl in the known compound by a formyl group (δ_H 9.37; δ_C 195.5) in **1**. The location of formyl group was assigned at C-8 by HMBC correlations from H_2-7 and H-9 to the aldehyde carbon C-19. Detailed 2D NMR analysis (HSQC, ^1H–^1H COSY, and HMBC) further supported the planar structure of **1** as depicted (Fig. 2).

The relative configuration of **1** was established by analysis of the NOESY data. The NOESY correlation of H_3-16/H_3-20 indicated that CH_3-20 and the isopropyl group were cofacial and designated as α-orientation. All of the Δ^4, Δ^8, and Δ^{13} double bonds were assigned as *E* geometry by NOESY correlations of H-6b/H_3-18, H-9/H-19, and H-1/H-13, respectively. The absolute configuration (1*R*,12*S*) of **1** was determined by the single-crystal X-ray crystallographic analysis using the CuKα radiation [Flack parameter = 0.06 (8)] (Fig. 4). Thus, **1** was determined as depicted and was given the trivial name euphoroylean A.

Compound **2** had a molecular formula $C_{20}H_{32}O_2$ as established by

Table 1
^{1}H NMR spectroscopic data of compounds **1–9** (δ in ppm, J in Hz).

No.	1[a]	2[a]	3[a]	4[a]	5[b]	6[a]	7[a]	8[a]	9[a]
1	1.69, m	1.21, m	6.12, s	6.07, s	5.93, s	*α* 1.61, m *β* 1.07, m	*α* 1.61, m *β* 1.07, m	*α* 2.01, m *β* 1.53, m	*α* 2.79, dd (14.9, 9.0) *β* 1.69, t (15.0)
2	*α* 1.27, m *β* 1.72, m	4.26, t (9.3)				a 1.65 b 1.54	a 1.66 b 1.55	*α* 2.38, ddd (15.9, 8.7, 6.9) *β* 2.61, m	2.48, m
3	2.00, m	5.31, d (9.7)	5.13, s	4.99, s	3.83, s	4.46, dd (11.6, 4.3)	4.46, dd (11.8, 4.4)		5.26, d (8.5)
4									
5	4.83, d (9.0)	a 2.35, m b 2.27,t (6.4)	5.54, s	5.24, s	5.43, s	0.90, m	0.90, m	1.68, m	5.54, br s
6	a 2.36, m b 2.00, m	2.52, m				*α* 1.38, m *β* 1.54, m	*α* 1.43, m *β* 1.52, m	a 1.73, m b 1.50, m	
7	2.23, td (11.9, 3.0)	6.47, dd (7.7, 5.4)	5.85, m	5.81, m	6.25, d (4.8)	*α* 0.91, m *β* 2.37, m	*α* 0.90, m *β* 2.35, m	1.53, m	5.10, d (2.0)
8			4.42, br d (11.9)	4.33, br d (11.8)	4.32, d (12.6)				3.55, dd (9.9, 6.1)
9	6.52, dd (9.9, 4.9)	2.35, m				1.59, m	1.56, m	1.19 d (7.9)	1.18, t (9.7)
10	a 2.68, m b 2.45, m	2.21, m							
11	a 2.00, m b 1.49, m	4.92, t (7.8)	2.58, m	2.51, m	2.46, m	*α* 1.69, m *β* 1.94, ddd (14.1, 11.5, 3.9)	*α* 1.78, m *β* 1.93, m	*α* 1.39, m *β* 1.55, m	1.02, m
12			*α* 1.86, m *β* 2.41, m	*α* 1.80, m *β* 2.37, m	*α* 1.79, m *β* 2.27, m	2.76, dd (6.3, 3.0)	2.78, dd (6.3, 2.9)	a 1.63, m b 1.52, m	4.89, dd (11.0, 4.0)
13	5.72, d (15.8)	1.89, t (8.9)	0.92, m	0.90, m	0.73, m	3.83, d (3.0)	4.99, d (3.0)	2.66, m	2.94, m
14	5.27, dd (15.8, 8.8)	a 1.34, m b 0.95, m	1.11, m	1.09, m	1.03, m			a 1.88, d (11.4) b 1.13, m	
15	1.46, m	2.07, m				2.27, s	2.33, m	2.07, s	
16	0.83, d (6.8)	0.86, d (6.9)	1.16, s	1.13, s	1.15, s				0.94, d (7.4)
17	0.87, d (6.8)	0.95, d (6.9)	a 4.33, d (11.9) b 4.26, d (11.9)	a 4.27, d (11.9) b 4.20, d (12.0)	1.06, s	a 4.98, s b 4.83, s	a 4.90, s b 4.80, s	a 4.82, s b 4.76, s	2.09, s
18	1.54, s	1.76, s	1.01, d (7.1)	0.98, d (7.2)	1.00, d (7.1)	0.86, s	0.87, s	1.27, s	1.09, s
19	9.37, s	9.35, s	1.78, s	1.75, s	1.84, s	0.82, s	0.83, s	a 3.97 b 3.42	1.09, s
20	1.42, s	1.50, s	1.55, s	1.54, s	a 5.55, d (12.5) b 4.32, d (12.6)	0.68, s	0.74, s	1.03, s	1.05, d (7.2)

[a] Measured at 400 MHz in $CDCl_3$.
[b] Measured at 500 MHz in $CDCl_3$.

the HRESIMS data. The 1D NMR data of **2** resembled those of a known cembrane diterpenoid, *epi*-mukulol (Bensemhoun et al., 2008), with the only difference being the replacement of a vinyl-methyl in *epi*-mukulol by a formyl group (δ_H 9.35; δ_C 195.3) in **2**. The location of the formyl group was assigned at C-19 by the key HMBC correlations from H-7 and H_2-9 to the aldehyde carbonyl (δ_C 195.3). This was further supported by the downfield-shifted C-8 signal in **2** with respect to that in *epi*-mukulol (δ_C 142.3 in **2**; δ_C 132.5 in *epi*-mukulol). The relative configuration of **2** was determined to be the same as that of *epi*-mukulol by comparison of their 1D NMR data and NOESY correlations. Specifically, the strong NOESY correlation of H-2/H-15 indicated that H-2 and the isopropyl group were cofacial, and were arbitrarily designated as *α*-orientation. The *trans*-relationship of H-1/H-2 was further supported by the large coupling constant of H-1/H-2 (J = 9.3 Hz) (Bensemhoun et al., 2008). The geometries of the Δ^3, Δ^7, and Δ^{11} double bonds were assigned as *E* by NOESY correlations of H_3-18/H-2, H-19/H-7, and H_3-20/H_2-10, respectively (Fig. 3).

The absolute configuration of C-2 in **2** was assigned by $Rh_2(OCOCF_3)_4$-induced CD analysis. On the basis of the bulkiness rule for secondary alcohols (Gerards and Snatzke, 1990), a positive Cotton effect around 330 nm in the $Rh_2(OCOCF_3)_4$-induced CD spectrum of **2** implied the *S*-configuration for C-2, allowing the determination of the absolute configuration of **2** as 1*S*, 2*S* (Fig. 5). This assignment was further supported by its similar specific rotation value with that of *epi*-mukulol ($[\alpha]_D$ +18.9 for **2**; $[\alpha]_D$ +21.2 for *epi*-mukulol), whose absolute configuration was verified by total synthesis (Reddy and Corey, 2018). Thus, **2** was determined as depicted and was named euphoroylean B.

Compound **3** was obtained as colorless gum, and its molecular formula was assigned as $C_{37}H_{44}O_8$ based on the HRESIMS ion peak at *m/z* 639.2928 (calcd for $C_{37}H_{44}O_8Na^+$, 639.2928). The ^{1}H and ^{13}C NMR data of **3** showed high similarity to those of a co-isolated known ingenane-type diterpenoid, (3*S*,4*S*,5*R*,8*S*,10*S*,11*R*,13*R*,14*R*,15*R*)-3*β*-*O*-angeloyl-17-tigloyloxy-20-deoxyingenol (**11**) (Wang et al., 2019), except for the presence of an additional benzoyl group in **3**, indicating **3** was a benzoylated derivative of **11**. The location of the benzoyl group was assigned at OH-5 by the HMBC correlation from H-5 (δ_H 5.54) to the benzoyl carbonyl (δ_C 166.6). This was further supported by the severely downfield-shifted H-5 signal in **3** with respect to that in **11** (δ_H 5.54 in **3**; δ_H 3.68 in **11**). The relative configuration of **3** was determined to be the same as that of **11** by comparison of their 1D NMR data and NOESY spectra. In particular, the NOESY cross-peak of H-3/H-5 assigned H-5 as *α*-oriented.

The absolute configuration of **3** was determined by comparison of its experimental and calculated electronic circular dichroism (ECD) spectra using the quantum chemical time-dependent density functional

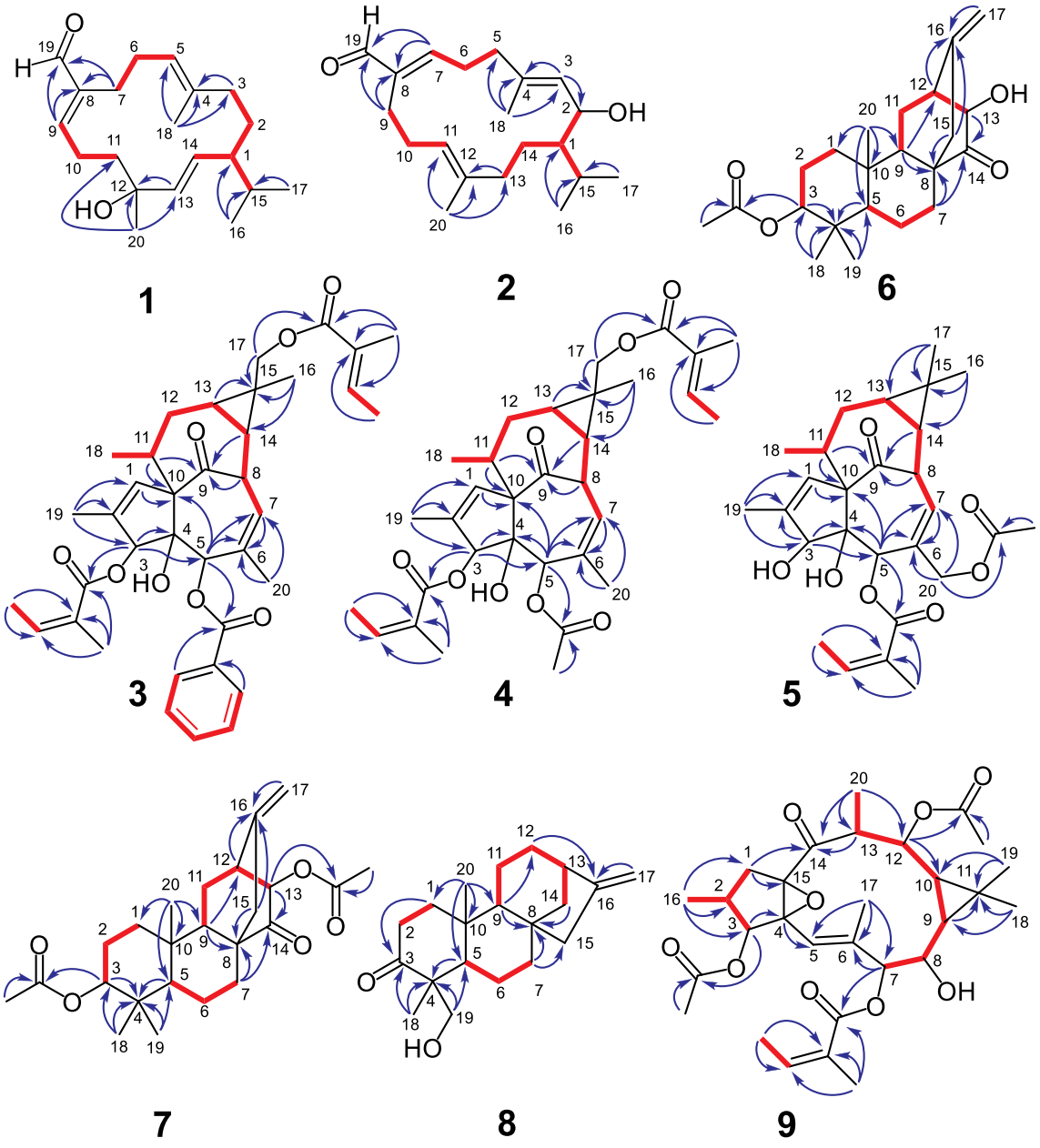

Fig. 2. Key ^{1}H–^{1}H COSY(——) and HMBC (⁀) correlations of **1** − **9**.

theory (TDDFT) method. As shown in Fig. 6, the experimental ECD spectrum of **3** showed Cotton effects around 238 nm (−), 217 nm (+), and 200 nm (+), respectively, which matched well with those calculated for the (3*S*,4*S*,5*R*,8*S*,10*S*,11*R*,13*R*,14*R*,15*R*)-isomer (**3a**), indicating that **3** possessed the same absolute configuration as **3a**. This assignment was consistent with the biogenetic origin of ingenane diterpenoids isolated from this genus. Thus, **3** was determined as depicted and was given the trivial name euphoroylean C.

Compound **4** had a molecular formula $C_{32}H_{42}O_8$ as established by HRESIMS data. The ^{1}H and ^{13}C NMR data of **4** resembled those of **11**, except for the presence of an additional acetyl group in **4**, indicating that **4** was an acetylated derivative of **11**. The location of acetyl group in **4** was assigned at OH-5 by the HMBC correlation from H-5 to the acetyl carbonyl (δ_C 171.2) (Fig. 2). This was further supported by the notable downfield-shifted H-5 signal in **4** with respect to that in **11** (δ_H 5.24 in **4**; δ_H 3.68 in **11**). Detailed 2D NMR analysis (HSQC, ^{1}H–^{1}H COSY, and HMBC) further supported the planar structure of **4** as depicted.

The configuration of **4** was determined to be the same with that of **11** by comparison of their 1D NMR data, NOESY spectra, and ECD spectra. The experimental ECD spectrum of **4** showed Cotton effects being around 201 nm (+) and 218 nm (+), matching well with those of **11** (Wang et al., 2019), which allowed the assignment of 3*S*,4*S*,5*R*,8*S*,10*S*,11*R*,13*R*,14*R*,15*R* configuration for **4**. Compound **4** was given the trivial name euphoroylean D.

Compound **5** had a molecular formula $C_{27}H_{36}O_7$ as established by HRESIMS data. The ^{1}H and ^{13}C NMR data of **5** showed high similarity to those of a known ingenane diterpenoid, ingenol (McKerrall et al., 2014), except for the presence of an additional angeloyl group and an acetyl group in **5**. The locations of the angeloyl and acetyl groups in **5** were assigned at OH-5 and OH-20, respectively, by the HMBC correlations from H-5 to the acetyl carbonyl (δ_C 170.9) and from H_2-20 to the angeloyl carbonyl (δ_C 167.1). This was further supported by the notable downfield-shifted H-5 and H_2-20 signals in **5** with respect to those in ingenol [δ_H 5.43 for H-5, δ_H 4.55–4.32 for H_2-20 in **5**; δ_H 4.40 for H-5, δ_H 4.15–4.06 for H_2-20 in ingenol].

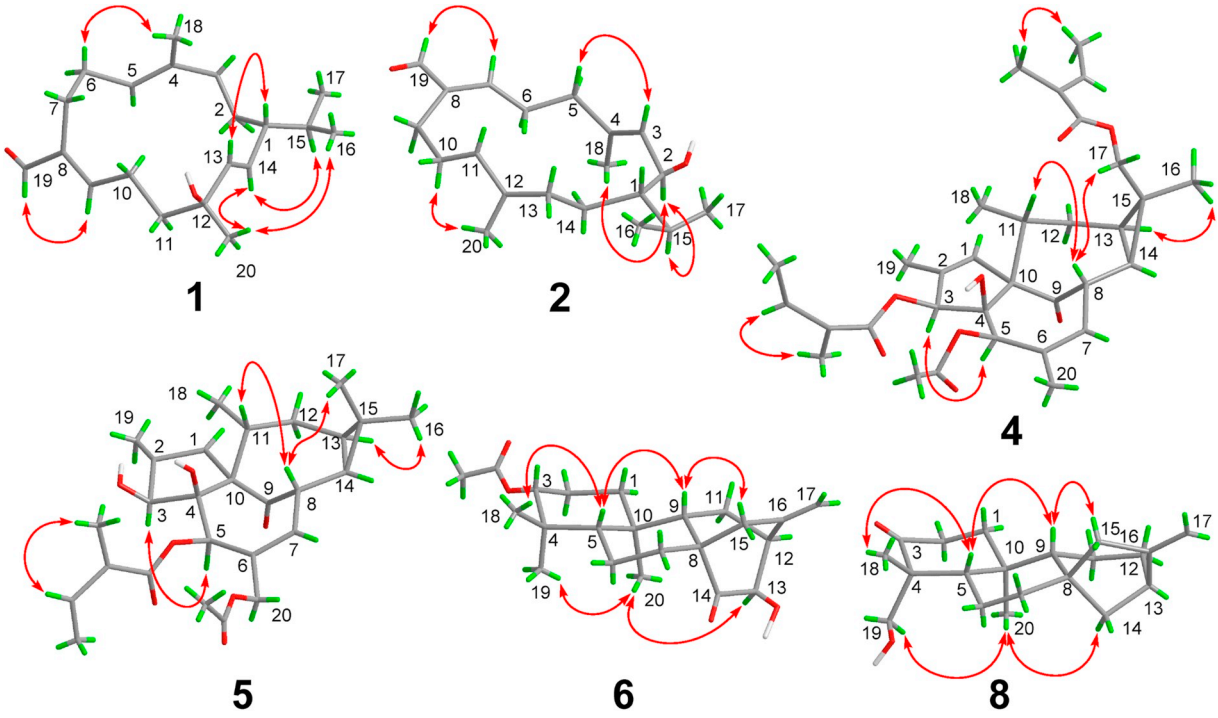

Fig. 3. Key NOESY correlations (↔) of compounds **1**, **2**, **4**, **5**, **6**, and **8**.

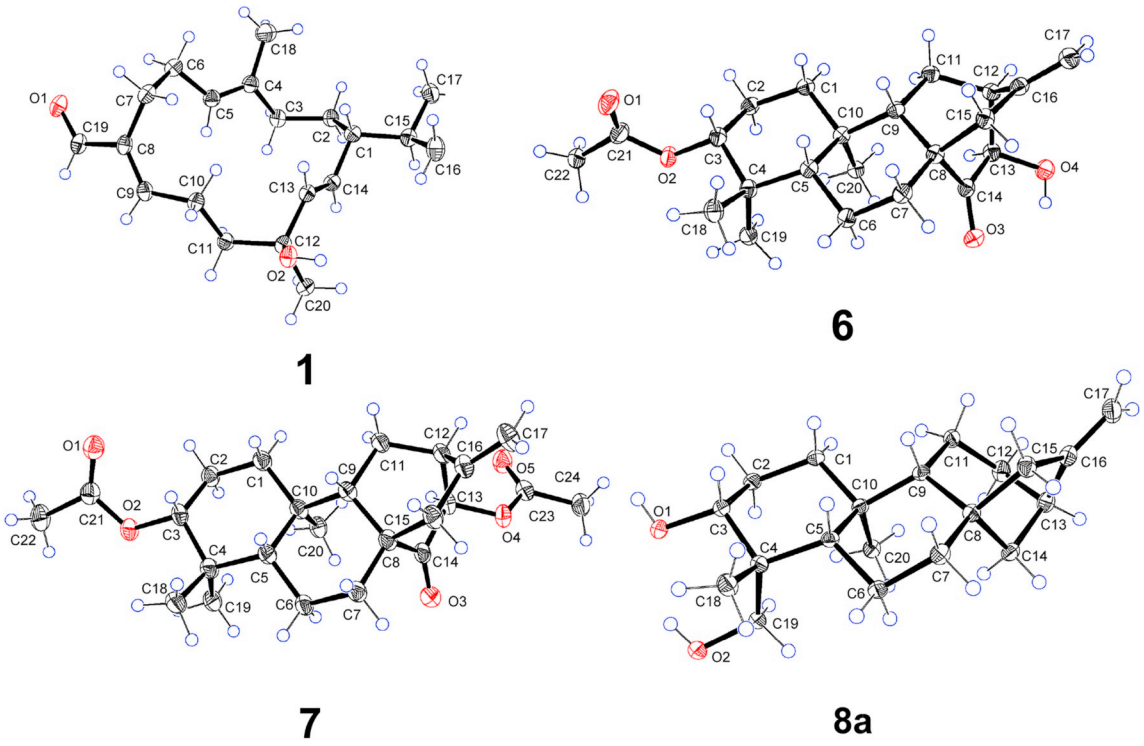

Fig. 4. Single-crystal X-ray structures of **1**, **6**, **7**, and **8a**.

The configuration of **5** was determined to be the same with that of ingenol by comparison of their 1D NMR data, NOESY spectra, and specific rotations. In particular, the NOE cross-peak of H-3/H-5 assigned H-5 as *α*-oriented. Since the absolute configuration of ingenol was determined by total synthesis (McKerrall et al., 2014), the similar specific rotation values of **5** and ingenol ($[\alpha]_D$ +52.0 for **5**; $[\alpha]_D$ +31.0 for ingenol), allowed the absolute configuration assignment of **5** as 3*S*,4*R*,5*R*,8*S*,10*S*,11*R*,13*R*,14*R*. This assignment was consistent with the biogenetic origin of ingenane diterpenoids isolated from this genus. Finally, **5** was determined as depicted and was given the trivial name euphoroylean E.

Compound **6** was isolated as colorless crystals. The molecular formula $C_{22}H_{32}O_4$ was established by HRESIMS data. The ^1H and ^{13}C NMR data of **6** showed high similarity to those of a known *ent*-atisane diterpenoid, *ent*-3*β*-(13*S*)-dihydroxyatis-16-*en*-14-one (Lal et al., 1990), except for the presence of an additional acetyl group in **6**, indicating

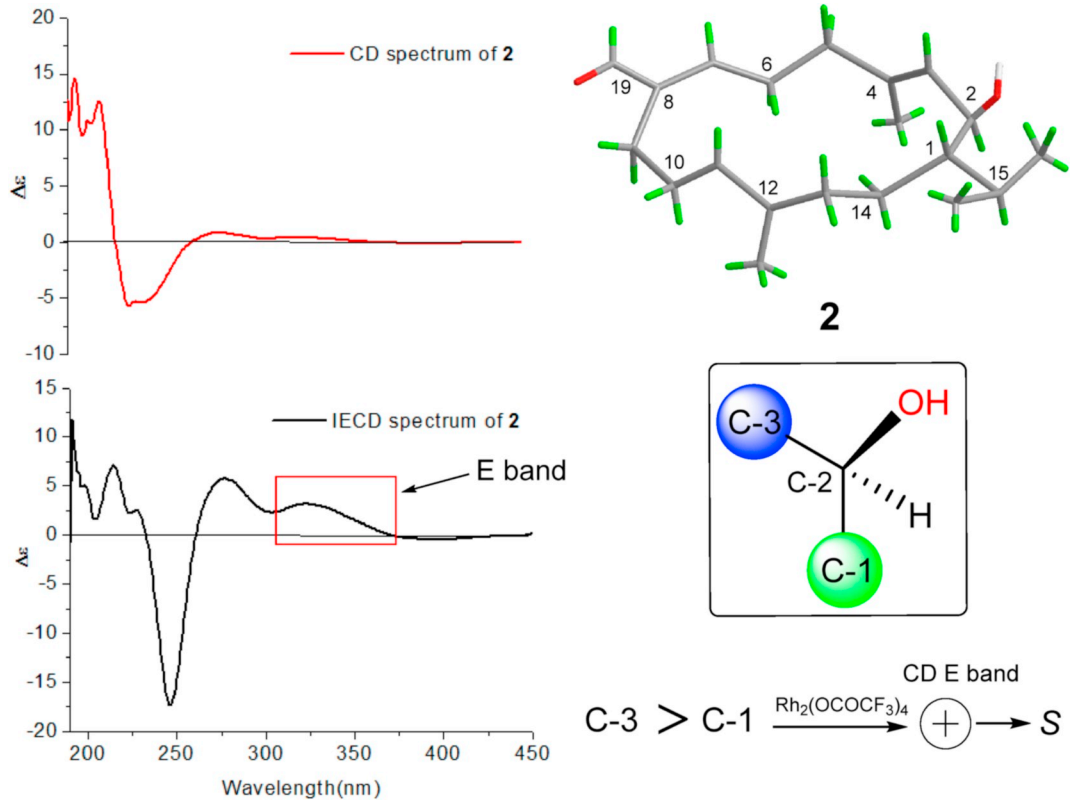

Fig. 5. Experimental CD spectrum (red line) of compound **2**, and the $Rh_2(OCOCF_3)_4$ induced CD spectrum (black line) of **2** in CH_2Cl_2 for 190–450 nm (left), and the applied bulkiness rule for secondary alcohols (right). (For interpretation of the references to color in this figure legend, the reader is referred to the Web version of this article.)

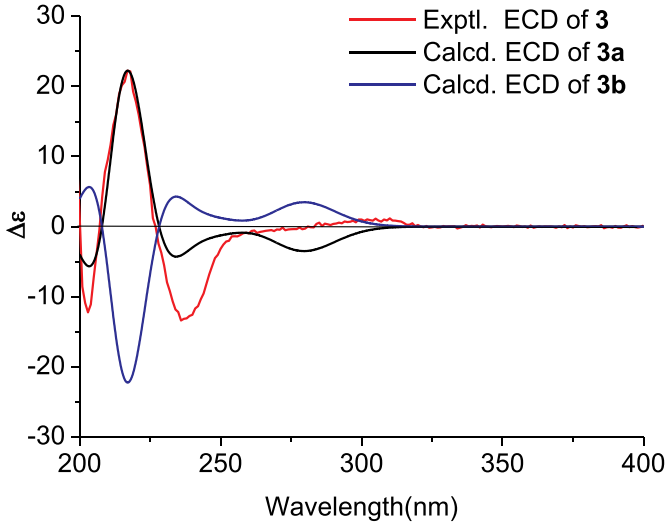

Fig. 6. Experimental ECD spectrum of **3** (red line) and calculated ECD spectra (200–400 nm) of (3*S*,4*S*,5*R*,8*S*,10*S*,11*R*,13*R*,14*R*,15*R*)-**3a** (black line) and (3*R*,4*R*,5*S*,8*R*,10*R*,11*S*,13*S*,14*S*,15*S*)-**3b** (blue line). (For interpretation of the references to color in this figure legend, the reader is referred to the Web version of this article.)

that **6** was the acetylated derivative of *ent*-3*β*-(13*S*)-dihydroxyatis-16-*en*-14-one. The location of the acetyl group was assigned at OH-3 by the HMBC correlation from H-3 to the acetyl carbonyl (δ_C 171.0). This was further supported by the downfield-shifted H-3 signal (δ_H 4.46) in **6** with respect to that in *ent*-3*β*-(13*S*)-dihydroxyatis-16-*en*-14-one (δ_H 3.21). Finally, the structure of **6** including the absolute configuration (3*S*,5*S*,8*S*,9*S*,10*R*,12*S*,13*R*) was secured by the X-ray single crystal diffraction analysis [Flack parameter = 0.05 (8)]. Compound **6** was given the trivial name euphoroylean F.

Compound **7** was isolated as colorless crystals. Its molecular formula $C_{24}H_{34}O_5$ was determined by HRESIMS data. The 1D NMR spectroscopic data of **7** were similar to those of **6**, with the only difference being the presence of an additional acetyl group in **7**, indicating that **7** was the acetylated derivative of **6**. The location of the acetyl group was assigned at OH-13 by the HMBC correlation from H-13 to the acetyl carbonyl (δ_C 170.4) (Fig. 2). This was further supported by the notable downfield-shifted H-13 signal in **7** with respect to that in **6** (δ_H 4.99 in **7**; δ_H 3.83 in **6**). The absolute configuration of **7** was also unambiguously confirmed as 3*S*,5*S*,8*S*,9*S*,10*R*,12*S*,13*R* by the X-ray single crystal diffraction analysis [Flack parameter = −0.03 (8)]. Compound **7** was given the trivial name euphoroylean G.

Compound **8** was isolated as colorless oil. The molecular formula $C_{20}H_{30}O_2$ was determined by HRESIMS data. The spectroscopic data of **8** resembled those of a known *ent*-kaurane diterpenoid, *ent*-18-hydroxykaur-16-*en*-15-one (Fraga et al., 1996), with the major difference being the different locations of the ketocarbonyl groups in these compounds. The ketocarbonyl group was assigned at C-3 in **8** rather than at C-15 in the known compound by the HMBC correlations from H_3-18 and H_2-19 to the ketocarbonyl (δ_C 222.0). This was also supported by the downfield-shifted C-2 (δ_C 34.4) and C-4 (δ_C 50.5) signals in **8** with respect to that in *ent*-18-hydroxykaur-16-*en*-15-one (δ_C 17.6 for C-2 and δ_C 37.4 for C-4). The relative configuration of **8** was determined to be the same with that of *ent*-18-hydroxykaur-16-*en*-15-one by comparison of their 1D NMR data and NOESY spectra.

The absolute configuration of **8** was determined as 4*R*,5*S*,8*S*,9*R*,10*S*,13*R* by X-ray single crystal diffraction analysis of its C-3 reduced derivative **8a** [Flack parameter = −0.04 (7)]. **8a** was reported as a natural product in 1980 (Piozzi et al., 1980), but its absolute configuration (3*R*,4*R*,5*S*,8*S*,9*R*,10*S*,13*R*) was assigned for the first time

Table 2
^{13}C NMR spectroscopic data of compounds **1–9** (δ in ppm).

No.	1[a]	2[a]	3[a]	4[a]	5[b]	6[a]	7[a]	8[a]	9[a]
1	47.1, CH	50.4, CH	132.1, CH	132.0, CH	129.4, CH	36.2, CH_2	36.3, CH_2	39.1, CH_2	31.6, CH_2
2	27.9, CH_2	70.1, CH	136.2, C	135.8, C	139.6, C	23.4, CH_2	23.4, CH_2	34.4, CH_2	29.2, CH
3	37.1, CH_2	128.9, CH	82.6, CH	82.1, CH	79.8, CH	80.7, CH	80.7, CH	222.0, C	76.7, CH
4	133.6, C	137.7, C	86.2, C	85.8, C	85.5, C	37.7, C	37.7, C	50.5, C	73.6, C
5	124.0, CH	38.8, CH_2	77.4, CH	77.4, CH	74.7, CH	54.8, CH	54.8, CH	55.1, CH	116.8, CH
6	25.4, CH_2	29.3, CH_2	135.4, C	135.0, C	133.9, C	18.8, CH_2	18.8, CH_2	19.0, CH_2	140.5, C
7	24.2, CH_2	156.3, CH	125.4, CH	125.5, CH	132.0, CH	30.8, CH_2	31.2, CH_2	40.3, CH_2	80.2, CH
8	142.2, C	142.3, C	43.2, CH	43.0, CH	44.4, CH	47.5, C	48.0, C	44.0, C	69.9, CH
9	156.0, CH	24.6, CH_2	205.8, C	205.7, C	206.6, C	52.0, CH	51.8, CH	54.5, CH	29.7, CH
10	24.4, CH_2	24.9, CH_2	72.2, C	72.0, C	73.6, C	37.8, C	37.9, C	38.3, C	19.2, C
11	42.7, CH_2	122.6, CH	38.8, CH	38.8, CH	39.1, CH	25.4, CH_2	25.5, CH_2	21.0, CH_2	31.3, CH
12	72.6, C	137.0, C	31.0, CH_2	30.9, CH_2	31.6, CH_2	45.0, CH	43.3, CH	32.9, CH_2	71.0, CH
13	136.9, CH	40.3, CH_2	24.0, CH	24.0, CH	23.7, CH	75.2, CH	74.9, CH	43.8, CH	43.1, CH
14	130.8, CH	25.3, CH_2	23.8, CH	23.6, CH	23.3, CH	218.3, C	212.2, C	39.2, CH_2	207.8, C
15	32.6, CH	27.7, CH	28.1, C	28.0, C	24.0, C	44.0, CH_2	43.3, CH_2	48.7, CH_2	71.2, C
16	19.9, CH_3	21.5, CH_3	24.5, CH_3	24.5, CH_3	15.8, CH_3	142.7, C	142.4, C	155.1, C	17.1, CH_3
17	20.4, CH_3	17.6, CH_3	65.9, CH_2	65.8, CH_2	28.6, CH_3	111.0, CH_2	110.5, CH_2	103.6, CH_2	18.0, CH_3
18	14.7, CH_3	17.2, CH_3	16.7, CH_3	16.6, CH_3	18.1, CH_3	28.5, CH_3	28.5, CH_3	22.7, CH_3	29.6, CH_3
19	195.5, C	195.2, C	15.6, CH_3	15.6, CH_3	15.4, CH_3	16.8, CH_3	16.9, CH_3	65.9, CH_2	16.7, CH_3
20	28.0, CH_3	15.6, CH_3	21.4, CH_3	21.3, CH_3	66.8, CH_2	14.2, CH_3	14.0, CH_3	18.8, CH_3	13.5, CH_3

[a] Measured at 100 MHz in $CDCl_3$.
[b] Measured at 125 MHz in $CDCl_3$.

in the current study. Compound **8** was given the trivial name euphoroylean H.

Compound **9** was a known ingol diterpenoid previously isolated from *Euphorbia nivulia* (Ravikanth et al., 2003). However, some of its NMR data were misassigned. In the current study, the ^{1}H NMR signals of H-1α and H-1β were revised to δ_H 2.79 and 1.69, respectively, while the ^{13}C NMR signals at C-7 and C-12 were revised to δ_C 80.2 and 71.0, respectively (Tables 1 and 2).

The known compounds quorumolide C (**10**) (Qi et al., 2018), (3*S*,4*S*,5*R*,8*S*,10*S*,11*R*,13*R*,14*R*,15*R*)-3β-*O*-angeloyl-17-tigloyloxy-20-deoxyingenol (**11**) (Wang et al., 2019), 20-acetyl-ingenol-3-angelate (**12**), 3-angelate- 20-hydroxyl-ingenol (**13**) (Marco et al., 1997), (3*S*,4*S*,5*R*,8*S*,10*S*,11*R*,13*R*,14*R*,15*R*) -3β-*O*-angeloyl-17-benzoyloxy-20-deoxyingenol (**14**) (Wang et al., 2019), ingol-3,7,12-triacetate-8-benzoate (**15**) (Marco et al., 1997), ingol-3,8,12-triacetate-7-tiglate (**16**) (Connolly et al., 1984), 3,7,12-*O*-triacetyl-8-*O*-(2-methylbutanoyl)-ingol (**17**) (Baloch et al., 2006), euphorantins M (**18**) (Qi et al., 2014), 3,12-di-*O*-acetyl-8-*O*-tigloyl-ingol (**19**) (Ahmed et al., 1999), 8-*O*-methyl-ingol-3,12-diacetate-7-benzoate (**20**) (Connolly et al., 1984), 3,8,12-*O*-triacetylingol-7-benzoate (**21**) (Li et al., 2009), 8-*O*-methyl-ingol-3,8,12-triacetate-7-angelate (**22**) (Connolly et al., 1984), 3,12-diacetyl-8-benzoylingol (**23**) (Ravikanth et al., 2002), 8-*O*-methyl-ingol-12-acetate-7-angelate (**24**) (Connolly et al., 1984), *ent*-atis-16-ene-3,14-dione (**25**) (Lal et al., 1990), eurifoloid L (**26**), eurifoloid J (**27**), eurifoloid G (**28**), eurifoloid E (**29**) (Zhao et al., 2014), and antiquorine A (**30**) (Yan et al., 2018), were identified by comparison of their spectroscopic data with those in the literatures.

2.2. MDR chemoreversal abilities

All of the isolates were screened for their chemoreversal abilities on MDR cancer cell line HepG2/DOX. Firstly, the intrinsic cytotoxicities of **1 − 30** were evaluated using the MTT method, and all compounds showed no obvious cytotoxicity (IC_{50} > 50 μM) in HepG2 and HepG2/DOX cell lines, as well as in the normal cells LO2, HEK293, and NCM460 (Table 3 and Table S1). Then, the cell viability assay was performed by combination of 10 μM of tested compounds with 50 μM of DOX in HepG2/DOX. The first- and third-generation MDR modulators, verapamil (Vrp) and tariquidar (Tar), were used as positive controls. As a result (Fig. 7), eight lathyrane-type diterpenoids (**15–18** and **20–23**) exhibited comparable chemoreversal activitites to the positive drug Vrp. These active compounds were further combined with various concentrations of DOX to obtain the exact reversal folds (Table 3). Among them, ingol-3,7,12-triacetate-8-benzoate (**15**) was identified as the most active MDR modulator, which could enhance the efficacy of anticancer drug DOX to *ca.* 105 folds at 10 μM, being stronger than that of Vrp (reversal fold = 46.92).

As the high expression of P-gp is the primary mechanism in MDR, the expressions of P-gp in HepG2/DOX cells were tested. Unsurprisingly, the MDR cell line showed a significant higher expression of P-gp than its parental cell line (Fig. 8). Thus, the MDR reversal mechanism of the current diterpenoids might be related to the modulation of P-gp, either down-regulation of its expression or blockage of its function. Firstly, the effect of **15** on the expression of P-gp in HepG2/DOX cells was investigated. As shown in Fig. 8, after incubation of **15** with HepG2/DOX cells for 24 h, no significant change of the P-gp level was observed. The Rho-123 accumulation assay was used to evaluate the effects of **15** on the P-gp transport function. As shown in Fig. 9, **15** could effectively increase the intracellular accumulation of Rho-123 in a dose-dependent manner and interrupt its efflux in HepG2/DOX cells. Taken together, the aforementioned results indicated that **15** could inhibit the transport activity of P-gp rather than its expression.

2.3. Structure-activity relationships and molecular modeling

The different substitution patterns of these lathyrane diterpenoids made them a good set of homologues to evaluate structure–activity relationships. In general, the acylations of OH-3 and OH-8 were beneficial to the activity, as shown by **15 − 23** vs **9** and **24**. Furthermore, the presence of benzoyl group at C-7 or C-8 showed greater activity than angeloyl, tigloyl, or OMeBu groups, as shown by **20** vs **22**, **21** vs **16**, **15** vs **17**, and **23** vs **19** (Fig. 7 and Table 3).

To further explore the molecular recognition mechanism between the active diterpenoids and P-gp, **15** was subjected to silico analysis with human P-gp (PDB code: 6QEX). As shown in Fig. 10, **15** was docked well in the transmembrane domain (TMD) of P-gp. Three hydrogen bonds formed between 3-OAc and Tyr953, between 8-OBz and Gln-990, and between 14-C=O and Tyr310 were observed. The core structure could form hydrophobic forces with the aromatic and hydrophobic residues of the TMD pocket, including Ala229, Trp232, Phe303, Phe336, Leu339, Ile340, Phe343, Phe728, and Phe983, which favored the binding. This binding model could also be employed to

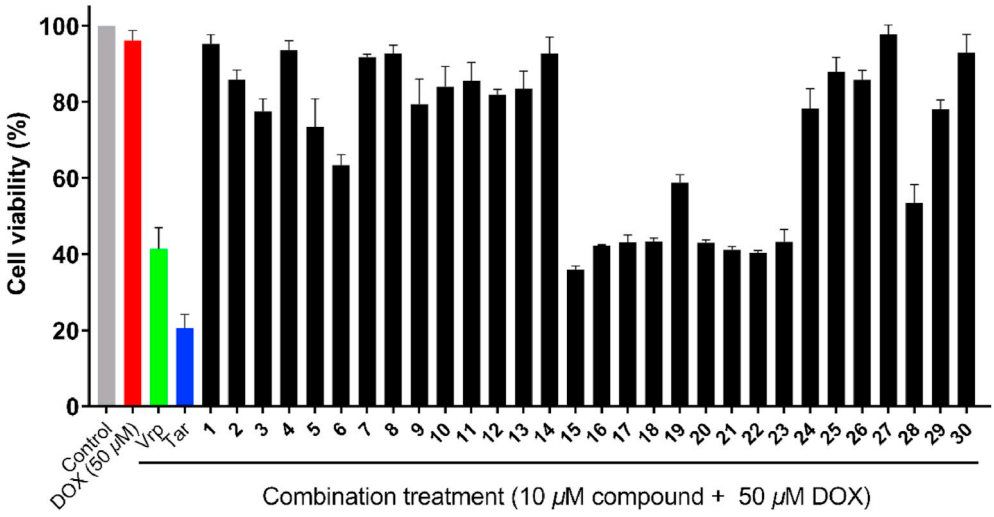

Fig. 7. Mediated multidrug resistance (MDR)-reversing effects of the compounds on doxorubicin (DOX)-resistant human hepatocellular carcinoma cell line (HepG2/DOX).

Table 3
Cytotoxicities and chemoreversal effects of the compounds (**15–18** and **21–23**).

Compounds	Cytotoxicity (IC_{50}, μM)		Combination treatment [a]	Reversal fold [b]
	HepG2/DOX	HepG2	IC_{50} (μM, mean ± SD)	
15	> 100	> 100	4.76 ± 0.93	105.11
16	> 100	> 100	27.29 ± 2.08	18.32
17	> 100	> 100	18.98 ± 2.83	26.33
18	> 100	> 100	20.81 ± 4.49	24.02
20	> 100	> 100	11.72 ± 2.06	42.65
21	> 100	> 100	11.18 ± 2.38	44.72
22	> 100	> 100	17.83 ± 2.88	28.02
23	> 100	> 100	26.45 ± 4.69	18.9
Vrp	> 100	> 100	10.65 ± 2.23	46.92
Tar	> 100	> 100	2.31 ± 0.21	216.25
Dox	499.88 ± 38.23	0.71 ± 0.14	NA	NA

[a] HepG2/DOX cells were treated with DOX in the presence of the 10 μM P-gp inhibitors.
[b] The reversal fold is calculated as a ratio of $IC_{50\ (DOX)}$ to $IC_{50\ (DOX+\ P\text{-}gp\ inhibitor)}$.

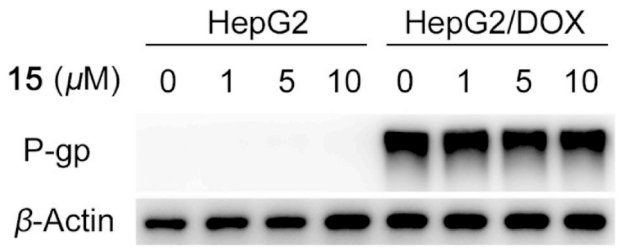

Fig. 8. Effects of **15** on the expression of P-gp.

explain the general structure-activity relationships (SARs) of the lathyrane diterpenoids (**9** and **15–24**). In general, the acylation of the free hydroxyls were beneficial to the activity, as the hydrophobicity was a key factor of a P-gp inhibitor targeting to the membrane protein. Specifically, the esterifications of OH-3 and OH-8 were essential to the activity, as the presence of free hydroxyls at these sites would sharply decrease the activity (**15–23** vs **9** and **24**). This was possibly due to the disruption of the hydrogen bond force. Furthermore, the presence of benzoyl group at OH-7 or OH-8 showed greater activity than angeloyl, tigloyl, or MeBu groups, as shown by **20** vs **22**, **21** vs **16**, **15** vs **17**, and **23** vs **19**. This was possibly due to stacking interaction of the phenyl ring in 8-OBz with the hydrophobic pocket formed by Trp232, Ala229, and Phe343, which favored the binding.

3. Conclusions

In our continuing investigation on MDR reversal agents from the Euphorbiaceae plants, eight previously undescribed diterpenoids, comprising four skeletal types, along with 22 known analogues were isolated from the whole plants of *E. royleana*. Among them, **1**, **2**, and **10** are the first cembrane examples from *E. royleana*.

Compound **15** was identified as a potent MDR modulator that could enhance the efficacy of DOX to *ca.* 105 folds at 10 μM. Mechanistic study indicated that **15** could inhibit the transport activity of P-gp rather than its expression, and the possible recognition mechanism between compounds and P-gp were predicted by molecular docking.

The current study not only enriched the chemical diversity of *Euphorbia* diterpenoids, but also provided a potential structural motif in future MDR reversal drug development.

4. Experimental section

4.1. General experimental procedures

Melting points were measured using an X-4 melting instrument and uncorrected. Optical rotations were determined on a Rudolph Autopol I automatic polarimeter. The UV spectra were determined on a Shimadzu UV-2450 spectrophotometer. IR spectra were determined in KBr disks on a Bruker Tensor 37 infrared spectrophotometer. NMR spectra were

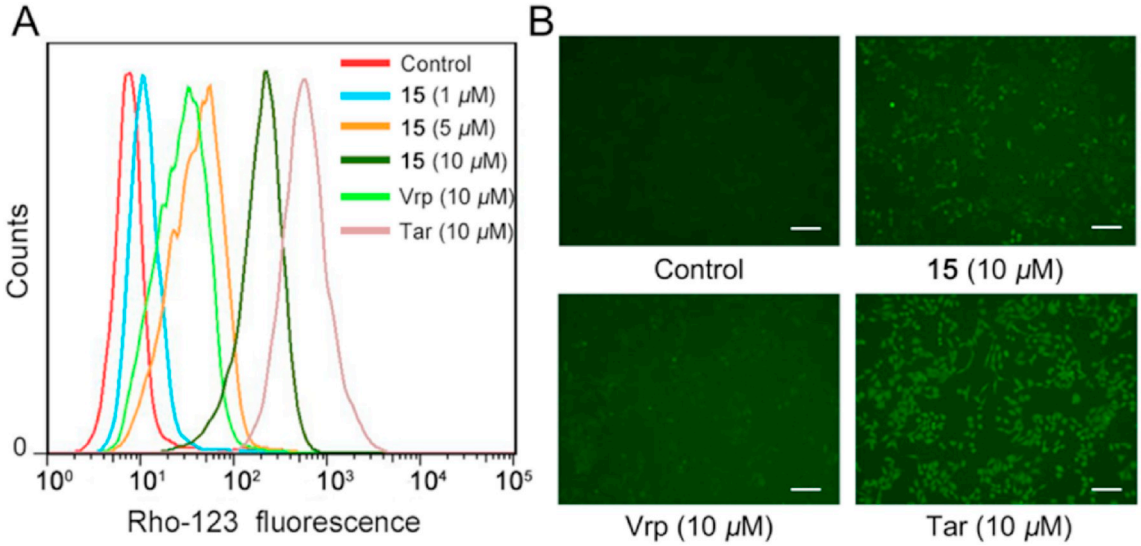

Fig. 9. (A) Inhibitory effects of **15** on the accumulation of rhodamin-123 (Rho-123) in HepG2/DOX. (B) Inhibitory effects of **15** on the efflux of Rho-123 in HepG2/DOX. Scale bar = 200 μm.

measured on Bruker AM-500 and AM-400 spectrometer. HRAPCIMS was performed on an Orbitrap-Fusion-Lumos spectrometer (Fusion Lumos, ThermoFisher, USA), HRESIMS were performed on a Waters Micromass Q-TOF spectrometer (Waters, Milford, MA, USA). Semi-preparative HPLC was performed with a Shimadzu LC-20 AT equipped with an SPD-M20A PDA detector. Purification by HPLC was obtained on an YMC-pack ODS-A column (250 × 10 mm, S-5 μm, 12 nm). A chiral column (Phenomenex Lux, cellulose-2, 250 × 10 mm, 5 μm) was used for chiral separation. Silica gel (100–200 and 300–400 mesh, Qingdao Haiyang Chemical Co., Ltd.), MCI gel (CHP20P, 75–150 μm, Mitsubishi Chemical Industries Ltd.), reversed-phase C18 (RP-C18) silica gel (12 nm, S-50 μm, YMC Co., Ltd.), and Sephadex LH-20 gel (Amersham Biosciences) were used for column chromatography (CC). All solvents (analytical grade) used were obtained from Guangzhou Chemical Reagents Company, Ltd. Annexin-V/FITC and Cell cycle were purchased from Keygen Biotech, China. MTT was purchased from Sigma, USA.

4.2. Plant material

The whole plants of *Euphorbia royleana* Boiss. (Euphorbiaceae) were collected in March 2019 from Yunnan province, P. R. China (N21°91′98.80″, E101°25′18.82″) and identified by Prof. You-Kai Xu of Xishuangbanna Tropical Botanical Garden, Chinese Academy of Sciences, and a voucher specimen (accession number: LD1903) was deposited at the School of Pharmaceutical Sciences, Sun Yat-sen University.

4.3. Isolation and extraction

The air-dried powder of *Euphorbia royleana* (10 kg) was extracted by 95% EtOH (3 × 5 L) at room temperature to give 900 g of crude extract, which was suspended in H_2O (3 L) and partitioned with petroleum ether (PE, 2 × 3 L), EtOAc (2 × 3 L) and *n*-BuOH (2 × 3 L). The PE fraction (400 g) was subjected to silica gel CC eluted with a PE/EtOAc gradient (30:1 → 1:1) to obtain four fractions (I − IV). Fr. III was separated by RP-18 silica gel CC (MeOH/H_2O, 50:50 → 100:0) to give four subfractions (III-a − III-d). Fr. III-b was separated by sephadex LH-20 and followed by HPLC equipped with a chiral column (MeCN/H_2O, 75:25, 3 mL/min) to yield **1** (15 mg, t_R 12.4 min) and **2** (4 mg, t_R 13.0 min). Fr. III-c was subjected to silica gel CC (PE/EtOAc, 20:1 → 1:1) to give three parts (III-c1 − III-c3). Fr. III-c1 was separated by Sephadex LH-20 and followed by semi-preparative HPLC (MeCN/H_2O, 65:35, 3 mL/min) to afford **10** (4 mg, t_R 13.3 min), **11** (20 mg, t_R

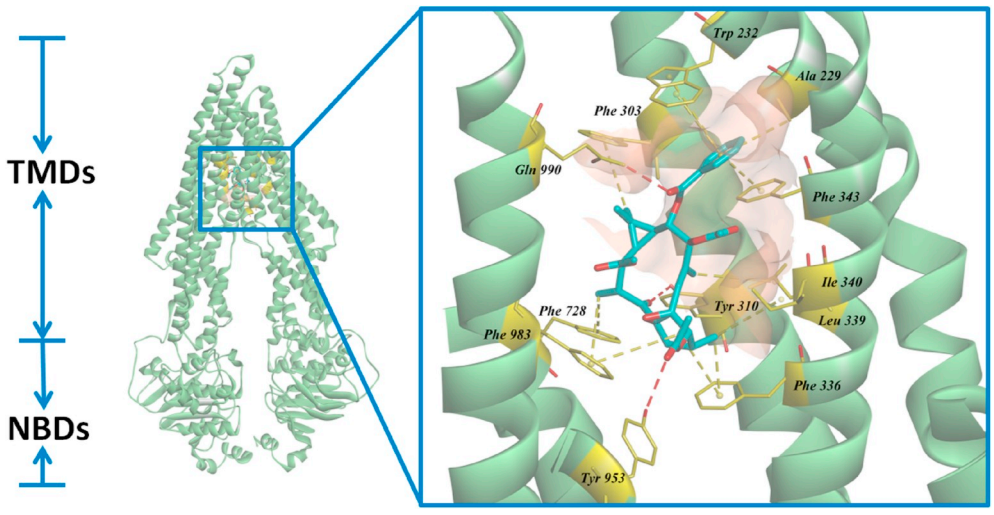

Fig. 10. Binding pose of **15** with human P-gp. The P-gp model was generated based on the PDB structure of human P-gp (Code: 6QEX) and was portrayed as a cartoon (light green). Residues involved in the interaction were colored yellow, while the surfaces of the hydrophobic pocket packing with **15** were colored light brown red. The hydrogen bonds and hydrophobic forces were shown as red dashed lines and yellow dashed lines, respectively. The structural figures were drawn in Accelrys Discovery Studio 2016. (For interpretation of the references to color in this figure legend, the reader is referred to the Web version of this article.)

16 min), **21** (10 mg, t_R 17 min), and **12** (20 mg, t_R 23 min). Fr. III-c3 was separated by Sephadex LH-20 and followed by semi-preparative HPLC (MeCN/H_2O, 85:15, 3 mL/min) to obtain **13** (10 mg, t_R 14.5 min), **16** (7 mg, t_R 21 min), **22** (5 mg, t_R 24 min), **23** (5 mg, t_R 26 min), and **14** (12 mg, 27 min). Fr. III-a was separated by silica gel CC (PE/EtOAc, 10:1) to afford **29** (130 mg), **17** (30 mg), **24** (10 mg), and **15** (14 mg). Fr. II was separated by MCI gel CC (MeOH/H_2O, 50:50 → 100:0) to obtain four fractions (Fr. II-a − Fr. II-d). Fr. II-b was separated by silica gel CC (PE/acetone, 20:1) to obtain three fractions (Fr. II-b1 − Fr. II-b3). Fr. II-b2 was purified by Sephadex LH-20 (MeOH) to give **6** (7 mg), **25** (12 mg), and followed by preparative TLC (CH_2Cl_2/MeOH, 100:1) to yield **5** (2 mg), **8** (18 mg), and **7** (4 mg). Fr. II-c was purified by Sephadex LH-20 (MeOH), and followed by semi-preparative HPLC (MeCN/H_2O, 80:20, 3 mL/min) to give **20** (40 mg, t_R 14.5 min), **9** (20 mg, t_R 16.3 min), **19** (9 mg, t_R 18.6 min), and **18** (9 mg, t_R 24.2 min). Fr. II-a was separated by silica gel CC (PE/EtOAc, 20:1), and followed by semi-preparative HPLC (MeCN/H_2O, 90:10, 3 mL/min) to afford **3** (17 mg, t_R 18 min), **4** (13 mg, t_R 21.6 min), and **26** (20 mg, t_R 25.2 min). Fr. II-d was separated by silica gel CC (PE/EtOAc, 25:1), and followed by semi-HPLC (MeCN/H_2O, 70:30, 3 mL/min) to afford **27** (10 mg, t_R 18 min), **28** (3 mg, t_R 21.6 min), and **30** (140 mg, t_R 25 min).

4.4. Spectroscopic data

Euphoroylean A (**1**): Colorless crystals; mp 168–170 °C; $[\alpha]_D^{23}$ −21.0 (*c* 0.10, MeCN); UV (MeCN) λ_{max} (log ε) 226 (1.31), 194 (1.75) nm; ECD (*c* 1.5 × 10^{-3} M, MeCN) λ_{max} ($\Delta\varepsilon$) 203 (+4.38), 216 (−6.18), 330 (+0.17) nm; IR (KBr) ν_{max} 3418, 2970, 2922, 1709, 1664, and 979 cm^{-1}; ^1H and ^{13}C NMR data see Tables 1 and 2; HRESIMS *m/z* 327.2289 $[M + Na]^+$ (calcd for 327.2295).

Euphoroylean B (**2**): Colorless oil; $[\alpha]_D^{23}$ +18.9 (*c* 0.10, MeCN); UV (MeCN) λ_{max} (log ε) 228 (2.36), 199 (2.80) nm; ECD (*c* 2.5 × 10^{-3} M, CH_2Cl_2) λ_{max} ($\Delta\varepsilon$) 195 (+14.6), 215 (+12.2), 220 (−5.80), 275 (+1.52) nm; IR (KBr) ν_{max} 3404, 2956, 2926, 1715, 1457, and 1080 cm^{-1}; ^1H and ^{13}C NMR data see Tables 1 and 2; HRESIMS *m/z* 327.2294 $[M + Na]^+$ (calcd for 327.2295).

Euphoroylean C (**3**): Colorless gum; $[\alpha]_D^{23}$ +55.0 (*c* 0.10, MeCN); UV (MeCN) λ_{max} (log ε) 222 (1.03), 196 (2.13) nm; ECD (*c* 2.5 × 10^{-3} M, MeCN) λ_{max} ($\Delta\varepsilon$) 204 (−11.50), 217 (+20.9), 238 (−13.50) nm; IR (KBr) ν_{max} 3362, 2956, 2921, 2852, 1713, 1651, 1451, 1381, 1252, and 709 cm^{-1}; ^1H and ^{13}C NMR data for the diterpene moiety see Tables 1 and 2; ^1H NMR data for acyloxy groups: 3-OAng [δ_H 6.03 (1H, qd, *J* = 7.1, 1.5), 1.82 (3H, d, *J* = 1.5), 1.86 (3H, t, *J* = 1.5)], 5-OBz [δ_H 8.20 (2H, d, *J* = 8.2), 7.49 (H, t, *J* = 7.8), 7.78 (2H, t, *J* = 7.4)], 17-OTig [δ_H 6.89 (1H, qd, *J* = 7.1, 1.3), δ_H 1.81 (3H, d, *J* = 1.3), δ_H 1.84 (3H, t, *J* = 1.3)]; ^{13}C NMR data for acyloxy groups: 3-OAng (δ_C 169.0, 127.5, 139.0, 20.8, and 15.8), 5-OBz (δ_C 166.6, 129.4, 130.5 × 2, 133.5, and 128.5 × 2), 17-OTig (δ_C 168.6, 132.1, 137.2, 14.5, and 12.2); HRESIMS *m/z* 639.2928 $[M + Na]^+$ (calcd for $C_{37}H_{44}O_8Na^+$ 639.2928).

Euphoroylean D (**4**): Colorless gum; $[\alpha]_D^{23}$ +74.0 (*c* 0.10, MeCN); UV (MeCN) λ_{max} (log ε) 218 (0.75), 197 (0.93) nm; ECD (*c* 2.5 × 10^{-3} M, MeCN) λ_{max} ($\Delta\varepsilon$) 201 (+10.5), 218 (+6.57) nm; IR (KBr) ν_{max} 3544, 2956, 2924, 2870, 2856, 1741, 1708, 1651, 1455, 1379, 1254, and 735 cm^{-1}; ^1H and ^{13}C NMR data for the diterpene moiety see Tables 1 and 2; ^1H NMR data for acyloxy groups: 3-OAng [δ_H 6.10 (1H, qd, *J* = 7.2, 1.5), 1.88 (3H, d, *J* = 1.5), and 1.97 (3H, t, *J* = 1.5)], 5-OAc [δ_H 2.29 (3H, s)], 17-OTig [δ_H 6.86 (1H, m), 1.80 (3H, d, *J* = 1.3), and 1.84 (3H, t, *J* = 1.3)]; ^{13}C NMR data for acyloxy groups: 3-OAng (δ_C 169.0, 127.6, 139.0, 20.9, and 16.0), 5-OAc (δ_C 171.2 and 21.0), 17-OTig (δ_C 168.6, 128.8, 137.2, 14.5, and 12.2); HRESIMS *m/z* 577.2770 $[M + Na]^+$ (calcd for $C_{32}H_{42}O_8Na^+$ 577.2772).

Euphoroylean E (**5**): Colorless gum; $[\alpha]_D^{23}$ +52.0 (*c* 0.10, MeCN); UV (MeCN) λ_{max} (log ε) 231 (1.12), 199 (2.61) nm; ECD (*c* 4.5 × 10^{-3} M, MeCN) λ_{max} ($\Delta\varepsilon$) 194 (+43.50), 218 (−13.5) nm; IR (KBr) ν_{max} 3405, 2932, 2854, 1738, 1704, 1658, 1455, 1377, 1259, and 763 cm^{-1}; ^1H and ^{13}C NMR data for the diterpene moiety see Tables 1 and 2; ^1H NMR data for acyloxy groups: 5-OAng [δ_H 6.15 (1H, qd, *J* = 7.2, 1.7), 1.92 (3H, d, *J* = 1.7), and 2.00 (3H, t, *J* = 1.7)], 20-OAc [δ_H 1.97 (3H, s)]; ^{13}C NMR data for acyloxy groups: 5-OAng (δ_C 167.1, 140.5, 127.1, 16.1, and 20.8), 20-OAc (δ_C 170.9, 21.0); HRESIMS *m/z* 495.2357 $[M + Na]^+$ (calcd for $C_{27}H_{36}O_7Na^+$ 495.2353).

Euphoroylean F (**6**): Colorless crystals; mp 208–210 °C; $[\alpha]_D^{23}$ +14.0 (*c* 0.10, MeCN); UV (MeCN) λ_{max} (log ε) 280 (0.12), 198 (2.49) nm; ECD (*c* 2.5 × 10^{-3} M, MeCN) λ_{max} ($\Delta\varepsilon$) 200 (+33.9), 218 (−13.6), 304 (+15.2) nm; IR (KBr) ν_{max} 3551, 2942, 2919, 2899, 1729, 1712, 1435, 1370, 1243, 1066, 1037, and 588 cm^{-1}; ^1H and ^{13}C NMR data for the diterpene moiety see Tables 1 and 2; ^1H and ^{13}C NMR data for acyloxy group: 3-OAc [δ_H 2.03 (3H, s), δ_C (171.0 and 21.4)]; HRESIMS *m/z* 383.2202 (calcd for $C_{22}H_{32}O_4Na^+$ 383.2193).

Euphoroylean G (**7**): Colorless crystals; mp 208–210 °C; $[\alpha]_D^{23}$ +21.0 (*c* 0.10, MeCN); UV (MeCN) λ_{max} (log ε) 280 (0.12), 198 (2.49) nm; ECD (*c* 2.5 × 10^{-3} M, MeCN) λ_{max} ($\Delta\varepsilon$) 200 (+8.1), 218 (−7.2), 304 (+11.8) nm; IR (KBr) ν_{max} 2926, 2874, 2853, 1746, 1729, 1438, 1369, 1229, 1054, 1028, and 584 cm^{-1}; ^1H and ^{13}C NMR data for the diterpene moiety see Tables 1 and 2; ^1H and ^{13}C NMR data for acyloxy groups: 3-OAc [δ_H 2.04 (3H, s), δ_C (171.1 and 21.4)], 13-OAc [δ_H 2.09 (3H, s), δ_C (170.4 and 21.0)]; HRESIMS *m/z* 425.2298 (calcd for $C_{24}H_{34}O_5Na^+$ 425.2298).

Euphoroylean H (**8**): Colorless oil; $[\alpha]_D^{23}$ +40.0 (*c* 0.20, MeCN); UV (MeCN) λ_{max} (log ε) 281 (0.07), 195 (1.55) nm; ECD (*c* 2.5 × 10^{-3} M, MeCN) λ_{max} ($\Delta\varepsilon$) 194 (−10.7) nm; IR (KBr) ν_{max} 3405, 2932, 2854, 1738, 1703, 1658, 1455, 1377, 1259 and 763 cm^{-1}; ^1H and ^{13}C NMR data see Tables 1 and 2, respectively; HRESIMS *m/z* 325.2138 $[M + Na]^+$ (calcd for $C_{20}H_{30}O_2Na^+$ 325.2138).

4.5. X-ray crystal structure analysis

Euphoroylean A (**1**): $C_{20}H_{32}O_2$ (*M* = 304.45 g/mol): monoclinic, space group C2 (no. 5), *a* = 19.8121(3) Å, *b* = 5.65430(10) Å, *c* = 17.8852(2) Å, β = 109.1400(10)°, *V* = 1892.81(5) $Å^3$, *Z* = 4, *T* = 99.99(10) K, μ(CuKα) = 0.513 mm^{-1}, *Dcalc* = 1.068 g/cm^3, 18677 reflections measured (5.23° ≤ 2Θ ≤ 153.942°), 3848 unique (R_{int} = 0.0353, R_{sigma} = 0.021. The final R_1 was 0.0329 (I > 2σ(I)) and wR_2 was 0.0912 (all data). Flack parameter = 0.06 (8). Crystallographic data for the structure of **1** have been deposited in the Cambridge Crystallographic Data Centre (deposition number: CCDC 1964466).

Euphoroylean F (**6**): $C_{22}H_{32}O_4$ (*M* = 360.47 g/mol): orthorhombic, space group $P2_12_12_1$ (no. 19), *a* = 7.39200(10) Å, *b* = 10.54680(10) Å, *c* = 23.7563(3) Å, *V* = 1852.09(4) $Å^3$, *Z* = 4, *T* = 100.01(10) K, μ(CuKα) = 0.694 mm^{-1}, D_{calc} = 1.286 g/cm^3, 18423 reflections measured (7.442° ≤ 2Θ ≤ 153.742°), 3840 unique (R_{int} = 0.0431, R_{sigma} = 0.0258). The final R_1 was 0.0392 (I > 2σ(I)) and wR_2 was 0.1092 (all data). Flack parameter = 0.05 (8). Crystallographic data for the structure of **6** have been deposited in the Cambridge Crystallographic Data Centre (deposition number: CCDC 1975522).

Euphoroylean G (**7**): $C_{24}H_{34}O_5$ (*M* = 402.51 g/mol): orthorhombic, space group $P2_12_12_1$ (no. 19), *a* = 7.45630(10) Å, *b* = 22.7182(3) Å, *c* = 25.0246(3) Å, *V* = 4239.01(9) $Å^3$, *Z* = 8, *T* = 100.01(10) K, μ(CuKα) = 0.698 mm^{-1}, *Dcalc* = 1.261 g/cm^3, 41602 reflections measured (5.254° ≤ 2Θ ≤ 153.986°), 8777 unique (R_{int} = 0.0664, R_{sigma} = 0.0443). The final R_1 was 0.0487 (I > 2σ(I)) and wR_2 was 0.1282. Flack parameter = −0.03 (8). Crystallographic data for the structure of **7** have been deposited in the Cambridge Crystallographic Data Centre (deposition number: CCDC 1975520).

Compound **8a**: Colorless crystals; mp 198–200 °C; $C_{20}H_{32}O_2$ (*M* = 304.45 g/mol): orthorhombic, space group $P2_12_12_1$ (no. 19), *a* = 7.53410(4) Å, *b* = 10.45115(6) Å, *c* = 21.16945(14) Å, *V* = 1666.884(18) Å3, *Z* = 4, *T* = 100.00(10) K, μ(CuKα) = 0.582 mm^{-1}, *Dcalc* = 1.213 g/cm^3, 17007 reflections

measured (8.354° ≤ 2Θ ≤ 153.498°), 3430 unique (R_{int} = 0.0318, R_{sigma} = 0.0206). The final R_1 was 0.0297 (I > 2σ(I)) and wR_2 was 0.0765 (all data). Flack parameter = −0.04 (7). Crystallographic data for the structure of **8a** have been deposited in the Cambridge Crystallographic Data Centre (deposition number: CCDC 1975558).

4.6. Determination of the absolute configuration of the secondary alcohol unit of compound 2

Compound **2** (0.5 mg) was dissolved in anhydrous CH_2Cl_2 (1 mL) and mixed with [$Rh_2(OCOCF_3)_4$] [molar ratio ca. 1:2 secondary alcohol/[$Rh_2(OCOCF_3)_4$]. After mixing, the first ECD spectrum of the mixture was measured immediately from 190 nm to 450 nm, and its time revolution was monitored until stable phase (about 30 min). The induced ECD (IECD) spectrum was subtracted from the inherent ECD spectrum. The observed sign of the band at around 330 nm in the induced CD spectrum is correlated to the absolute configuration of the secondary alcohol (Gerards and Snatzke, 1990).

4.7. Preparation of compound 8a

Compound **8** (12.00 mg) (M = 302.2246) was dissolved in methanol (2 mL) and treated with $NaBH_4$ (1.510 mg) at room temperature for 1 h. The mixture was diluted with 5 mL of H_2O, followed by the extraction of EtOAc (5 mL × 3). The organic layer was dried and evaporated to give a residue, which was purified by silica gel CC (PE/EtOAc, 10:1) to get **8a** (8.20 mg).

4.8. Cell culture

HepG2, HepG2/DOX, HEK239, LO2, and NCM460 cells were purchased from the Laboratory Animal Service Center at Sun Yat-sen University (Guangzhou, China). All cells were cultured in RPMI1640 culture medium (Gibco, USA) with 10% fetal bovine serum (Gibco, USA) and maintained in a 5% CO_2 incubator at 37 °C.

4.9. Cytotoxicity assay

Cells were seeded into 96-well plates (5 × 10^3 cells/well) for 24 h, and exposed to DOX with or without the tested for 48 h. The cells were incubated with 5 mg/mL MTT (Sigma, USA) for 4h, and the suspension was discarded. Subsequently, the dark blue crystals were solubilized in DMSO, and the absorbance of the solution was determined at 570 nm using a multifunction micro-plate reader.

4.10. Intracellular accumulation and efflux of Rho-123

The effects of compounds on the accumulation and efflux of Rho-123 in HepG2/DOX cells were investigated as previously described (Liu et al., 2019) with some modification. Briefly, HepG2/DOX cells were seeded into 12-well plates (3 × 10^5/well) for 24 h and incubated with the compounds (10 μM) for 2h, subsequently, incubated by Rho-123 (10 μM) in the dark at 37 °C for 1 h. The cells were rinsed three times with ice-cold PBS and harvested for flow cytometry analysis. For the efflux assay, the cells were incubated in medium containing 10 μM of Rho-123 for 1 h, and cultured in Rho-123-free medium with or without compounds for additional 2 h. Subsequently, the cells were rinsed three times with ice-cold PBS and photographed using fluorescence microscope. Tariquidar (Tar) and verapamil (Vrp) were used as the positive controls.

4.11. Western blot analysis

The cells were rinsed three times with ice-cold PBS buffer and lysed in RIPA buffer (Beyotime, China) containing protease inhibitor cocktails (Roche Life Science, USA). Total protein concentration was determined using a BCA protein assay kit (Beyotime, China). The cell lysates were mixed with sample dye (Beyotime, China) and boiled at 95 °C for 10 min. The prepared samples were resolved by SDS-PAGE electrophoresis and transfered to PVDF membrane. The blots were probed with specific antibodies (P-gp and GAPDH) and subsequently detected using enhanced chemiluminescence detection kit (Thermo, USA).

4.12. Molecular modeling

The complex model of compound **15** with P-gp was generated by Accelrys Discovery Studio 2016 software. The crystal structure of human P-gp in complex with the antigen-binding fragment of UIC2 (P-gp antibody) and taxol (PDB code: 6QEX) was used here for the docking studies. Hydrogen atoms and charges were added to the systems by using the CHARMm force field and the Momany-rone partial charge methods, and the crystallographic water molecules were removed. All ionizable residues in the systems were set to their protonation states at a neutral pH. Zosuquidar, the inhibitor of P-gp, was used as a reference compound to define the active site of 6QEX (Alam et al., 2019). The radius of the active site sphere was adjusted to 9 Å, and 10 random conformations were generated for each ligand by using CDOCKER. Other docking parameters were set to default values. And the reliability of this method was validated by the root-mean-square deviation (RMSD) values for the top 10 redocked poses of zosuquidar, which ranged from 0.8 to 2 Å relative to the crystal counterpart. Compared with the crystal pose, maintaining the RMSD of the best pose below the 1 Å threshold can be considered as a successful docking (Trost et al., 2003). Under identical conditions, **15** were docked into the 6QEX catalytic pocket, and the final posture of each ligand were ranged based on the "–CDOCKER_INTERACTION_ ENERGY" scores (Card et al., 2004).

Declaration of competing interest

The authors declare no competing financial interest.

Acknowledgments

This work was supported by Natural Science Foundation of China (81722042, 81973195, and 81973203) and Local Innovative and Research Teams Project of Guangdong Pearl River Talents Program (2017BT01Y093).

Appendix A. Supplementary data

Supplementary data to this article can be found online at https://doi.org/10.1016/j.phytochem.2020.112395.

References

Ahmed, A.A., Couladis, M., Mahmoud, A.A., de Adams, A., Mabry, T.J., 1999. Ingol diterpene ester from the latex of *Euphorbia lactea*. Fitoterapia 70, 140–143.

Alam, A., Kowal, J., Broude, E., Roninson, I., Locher, K.P., 2019. Structural insight into substrate and inhibitor discrimination by human P-glycoprotein. Sceince 363, 753–756.

Baloch, I.B., Baloch, M.K., Saqib, Q.N.U., 2006. Cytotoxic macrocyclic diterpenoid esters from *Euphorbia cornigera*. Planta Med. 72, 830–834.

Bensemhoun, J., Rudi, A., Bombarda, I., Gaydou, E.M., Kashman, Y., Aknin, M., 2008. Flexusines A and B and epimukulol from the soft coral *sarcophyton flexuosum*. J. Nat. Prod. 71, 1262–1264.

Bowden, B.F., Coll, J.C., Mitchell, S.J., Kazlauskas, R., 1981. Studies of Australian soft cocals. XXIV* two cembranoid diterpenes from the soft coral *Sinularia facile*. Aust. J. Chem. 34, 1551–1556.

Card, G.L., England, B.P., Suzuki, Y., Fong, D., Powell, B., Lee, B., Luu, C., Tabrizizad, M., Gillette, S., Ibrahim, P.N., Artis, D.R., Bollag, G., Milburn, M.V., Kim, S.H., Schlessinger, J., Zhang, K.Y.J., 2004. Structural basis for the activity of drugs that inhibit phosphodiesterases. Structure 12, 2233–2247.

Connolly, J.D., Fakunle, C.O., Rycroft, D.S., 1984. Five ingol esters and a 17-hydroxyigenol ester from the latex of *Euphorbia kamerunica*. Assignment of esters using ^{13}C N. M.R. methods. Tetrahedron Lett. 25, 3773–3776.

Flora of China Editorial Committee, 1997. Flora of China, vol. 44. Science Press, Beijing, pp. 62.
Fraga, B.M., González, P., Guillermo, R., Hernández, M.G., 1996. A study of the microbiological reduction of *α,β*-unsaturated carbonyl *ent*-kaurenes by *Gibberella fujikuroi*. Tetrahedron 52, 13767–13782.
Gerards, M., Snatzke, G., 1990. Circular dichroism, XCIII[1] determination of the absolute configuration of the alcohols, olefins, epoxides, and ethers from the CD of their "In Situ" complexes with $[Rh_2(OCOCF_3)_4]$. Tetrahedron: Asymmetry 4, 221–236.
Lal, A.R., Cambie, R.C., Rutledge, P.S., Woodgate, P.D., 1990. *Ent*-atisane diterpenes from *Euphorbia fidjiana*. Phytochemistry 29, 1925–1935.
Li, W., Tang, Y.Q., Sang, J., Tang, G.H., Yin, S., 2020. Jatrofolianes A and B, two highly modified lathyrane diterpenoids from *Jatropha gossypiifolia*. Org. Lett. 22, 106–109.
Li, X.L., Li, Y., Wang, S.F., Zhao, Y.L., Liu, K.C., Wang, X.M., Yang, Y.P., 2009. Ingol and ingenol diterpenes from the aerial parts of *Euphorbia royleana* and their anti-angiogenic activities. J. Nat. Prod. 72, 1001–1005.
Liu, C.P., Xie, C.Y., Zhao, J.X., Ji, K.L., Lei, X.X., Sun, H., Lou, L.G., Yue, J.M., 2019. Dysoxylactam A: a macrocyclolipopeptide reverses P-glycoprotein-mediated multidrug resistance in cancer cells. J. Am. Chem. Soc. 141, 3812–3816.
Marco, A.J., Sanz-Cervera, J.F., Yuste, A., 1997. Ingenane and lathyrane diterpenoids from the latex of *Euphorbia canariensis*. Phytochemistry 45, 563–570.
McKerrall, S.J., Jørgensen, L., Kuttruff, C.A., Ungeheuer, F., Baran, P.S., 2014. Development of a concise synthesis of (+)-ingenol. J. Am. Chem. Soc. 136, 5799–5810.
Piozzi, F., Savona, G., Hanson, J.R., 1980. Kaurenoid diterpenes from *Stachys lanata*. Phytochemistry 19, 1237–1238.
Qi, W.Y., Zhao, J.X., Wei, W.J., Gao, K., Yue, J.M., 2018. Quorumolides A−C, three cembranoids from *Euphorbia antiquorum*. J. Org. Chem. 83, 1041–1045.
Qi, W.Y., Zhang, W.Y., Shen, Y., Leng, Y., Gao, K., Yue, J.M., 2014. Ingol-type diterpenes from *Euphorbia antiquorum* with mouse 11*β*-hydroxysteroid dehydrogenase type 1 inhibition activity. J. Nat. Prod. 77, 1452–1458.
Ravikanth, V., Niranjan Reddy, V.L., Prabhakar Rao, T., Diwan, P.V., Ramakrishna, S., Venkateswarlua, Y., 2002. Macrocyclic diterpenes from *Euphorbia nivulia*. Phytochemistry 59, 331–335.
Ravikanth, V., Niranjan Reddy, V.L., Vijender Reddy, A., Ravinder, K., Prabhakar Rao, T., Siva Ram, T., Anand Kumar, K., Prakesh Vamanarao, D., Venkateswarlu, Y., 2003. Three new ingol diterpenes from *Euphorbia nivulia*: evaluation of cytotoxic activity. Chem. Pharm. Bull. 51, 431–434.
Reddy, D.S., Corey, E.J., 2018. Enantioselective conversion of oligoprenol derivatives to macrocycles in the germacrene, cembrene, and 18-membered cyclic sesterterpene series. J. Am. Chem. Soc. 140, 16909–16913.
Sarkadi, B., Homolya, L., Szakács, G., Váradi, A., 2006. Human multidrug resistance ABCB and ABCG transporters: participation in a chemoimmunity defense system. Physiol. Rev. 86, 1179–1236.
Shi, Q.W., Su, X.H., Kiyota, H., 2008. Chemical and pharmacological research of the plants in genus *Euphorbia*. Chem. Rev. 108, 4295–4327.
Trost, B.M., Toste, F.D., Greenman, K., 2003. Atom economy. Palladium-catalyzed formation of coumarins by addition of phenols and alkynoates via a net C−H insertion. J. Am. Chem. Soc. 125, 4518–4526.
Vasas, A., Hohmann, J., 2014. *Euphorbia* diterpenes: isolation, structure, biological activity, and synthesis (2008−2012). Chem. Rev. 114, 8579–8612.
Wang, P.X., Xie, C.F., An, L.J., Yang, X.Y., Xi, Y.R., Yuan, S., Zhang, C.Y., Tuerhong, M., Jin, D.Q., Lee, D., Zhang, J., Ohizumi, Y., Xu, J., Guo, Y.Q., 2019. Bioactive diterpenoids from the stems of *Euphorbia royleana*. J. Nat. Prod. 82, 183–193.
Yan, S.L., Li, Y.H., Chen, X.Q., Liu, D., Chen, C.H., Li, R.T., 2018. Diterpenes from the stem bark of *Euphorbia neriifolia* and their in *vitro* anti-HIV activity. Phytochemistry 145, 40–47.
Zhao, J.X., Liu, C.P., Qi, W.Y., Han, M.L., Han, Y.S., Wainberg, M.A., Yue, J.M., 2014. Eurifoloids A−R, structurally diverse diterpenoids from *Euphorbia neriifolia*. J. Nat. Prod. 77, 2224–2233.
Zhang, Y., Fan, R.Z., Sang, J., Tian, Y.J., Chen, J.Q., Tang, G.H., Yin, S., 2020. Ingol diterpenoids as P-glycoprotein-dependent multidrug resistance (MDR) reversal agents from *Euphorbia marginata*. Bioorg. Chem. 95, 103546–103556.
Zhu, J.Y., Wang, R.M., Lou, L.L., Li, W., Tang, G.H., Bu, X.Z., Yin, S., 2016. Jatrophane diterpenoids as modulators of P-glycoprotein-dependent multidrug resistance (MDR): advances of structure-activity relationships and discovery of promising MDR reversal agents. J. Med. Chem. 59, 6353–6369.